LiftWEC

DEVELOPMENT OF A NEW CLASS OF WAVE ENERGY CONVERTER BASED ON HYDRODYNAMIC LIFT FORCES

Deliverable D6.4

Fatigue assessment

Deliverable Lead	University of Strathclyde
Delivery Date	31st May 2022
Dissemination Level	Public
Status	Final
Version	1.3

This project has received funding from the European Union's Horizon 2020 research and innovation programme under grant agreement No 851885. This output reflects the views only of the author(s), and the European Union cannot be held responsible for any use which may be made of the information contained therein.

Document Information

Project Acronym	LiftWEC
Project Title	Development of a new class of wave energy converter based on hydrodynamic lift forces
Grant Agreement Number	851885
Work Package	WP06
Related Task(s)	T6.4
Deliverable Number	D6.4
Deliverable Name	Fatigue assessment
Due Date	31th May 2022
Date Delivered	31th May 2022
Primary Author(s)	Abel Arredondo-Galeana (AAG)
Co-Author(s)	Weichao Shi (WS), Feargal Brennan (FB)
Document Number	LW-D06-04

Version Control

Revision	Date	Description	Prepared By	Checked By
1.0	1/03/2022	Internal working draft	AAG	WS, FB
1.1	10/04/2022	Internal draft for review	AAG	WS, FB
1.2	16/05/2022	Draft for consortium Review	AAG	WS, FB
1.3	31/05/2022	Submission to EU	AAG	WS, FB

This project has received funding from the European Union's Horizon 2020 research and innovation programme under grant agreement No 851885. This output reflects the views only of the author(s), and the European Union cannot be held responsible for any use which may be made of the information contained therein.

EXECUTIVE SUMMARY

This document constitutes Deliverable '*D6.4 Fatigue assessment*" of the LiftWEC project. LiftWEC is a collaborative research project funded by the European Union's Horizon 2020 Research and Innovation Programme under Grant Agreement No 851885. It is the intention of the project consortium that the LiftWEC project culminates in the development of one or more promising configurations of a Wave Energy Converter operating through the use of one or more rotating hydrofoils that generate lift as the primary interaction with the incident waves.

In this report, a fatigue assessment is carried out on LiftWEC. The analysis is performed first through stress-life approaches in irregular sea-states. Firstly, damage is quantified through a probabilistic approach. It is assumed that LiftWEC operates at constant velocity which is equal to the peak frequency of a JONSWAP wave energy spectrum. Secondly, the damage quantified through the conventional time deterministic approach is compared to that computed through the probabilistic approach, yielding satisfactory results.

Critical areas of stress concentration are defined as "hot-spots". In this report, we illustrate the damage computation methodology in one hot-spot. The hotspot is the fixed end of the foil for a rotor with the foil supported at both ends. We demonstrate the effect of passive structural dynamics in the damage that occurs in this hot spot. This is with the aim to develop methods that retard or avoid complete structural failure.

We compare the damage and power output in different sea states. Although, it is expected that more power translates into more damage, it is found that this is not the case in the selected hot spot. This is because power is a function of the tangential force, whilst the damage is a function of the radial force imposing the bending moments on the hydrofoils.

In terms of structural dynamics and their impact in the damage of the hot spot, it is found that passive compliance of the support structure and passive radial motion of a single foil do not alter significantly the power and damage footprints of the hot spot when the device is operated with constant speed in irregular seas. In contrast, it is found that a passively pitching foil can help in reducing the damage on the hot spot, although incurred at a penalty in power production.

It is the intention of this deliverable to provide guidance and a methodology to assess the fatigue life of a LiftWEC device, by utilising realistic sea-state simulations. This can help in designing strategies for coping with load variability and extending the fatigue life of certain components through passive or active actuation.

This project has received funding from the European Union's Horizon 2020 research and innovation programme under grant agreement No 851885. This output reflects the views only of the author(s), and the European Union cannot be held responsible for any use which may be made of the information contained therein.

TABLE OF CONTENTS

This project has received funding from the European Union's Horizon 2020 research and innovation programme under grant agreement No 851885. This output reflects the views only of the author(s), and the European Union cannot be held responsible for any use which may be made of the information contained therein.

1 INTRODUCTION

Structural failure can occur in different modes. Static failure occurs through buckling or yielding, whilst dynamic failure occurs through impact or fatigue [1]. As such, it is important to characterise structures under different types of loading. In this work, we focus on the operational dynamic loading that LiftWEC could encounter during operation. As such, we focus on fatigue as a mode of structural failure. We recall that because LiftWEC operates in a submerged manner, impact loading is not expected during operation.

The definition of fatigue is the cumulative structural damage of a material under repeated or oscillatory loading whose magnitude would typically be insufficient to cause ultimate structural failure due to a singular application [2]. Hence, fatigue is a dynamic process that happens over time. The analysis of fatigue can allow operators to design control strategies that can help in coping with load variability via active or passive actuation. Some of these strategies will be studied in this deliverable.

1.1 LIFTWEC CONFIGURATIONS

At this stage of the LiftWEC project, four baseline LiftWEC configurations have been selected in the consortium: 1) monopile, 2) spar buoyed, 3) trifloater and 4) tensioned legged platform. Here we model the tensioned leg system as a v-frame structure. The configurations are depicted in Figure 1. We note that although some of the support structural dynamics of these structures will differ, the fatigue behaviour of the main rotor components (i.e. foils, lateral spokes, central shaft) will remain similar between the devices. As such, in this deliverable we will select a region of localised stresses which is common to the four devices, namely, the fixed end of the foils. We note that the methodology developed in this deliverable will be applicable to any other stress hotspot of any LiftWEC prototype, as long as a time series of bending stresses is available for that particular hot spot. Loading propagation cases from the foils to the rest of the substructures can be found, for example, in LW-D06-01-1x3 Extreme Event LiftWEC ULS Assessment [3].

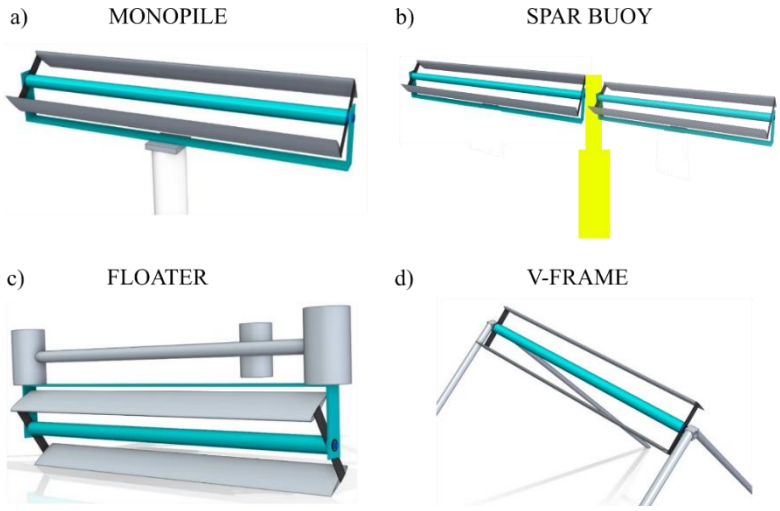

Figure 1 LiftWEC configurations supported by a) monopile, b) spar buoy, c) trifloater and d) v-frame

This project has received funding from the European Union's Horizon 2020 research and innovation programme under grant agreement No 851885. This output reflects the views only of the author(s), and the European Union cannot be held responsible for any use which may be made of the information contained therein.

2 METHODOLOGY

2.1 TIME DOMAIN METHODS

Fatigue analysis methods vary depending on the type of load applied to a structure. For constant loading, the SN relationship is defined by S, which is the constant amplitude stress range and N, which is the number of cycles to failure. As an example of uniform amplitude stress, we plot in Figure 2a the bending stresses on a fixed end of the foil for the case of a LiftWEC foil in regular waves. The foil cross-section corresponds to a NACA 0012 profile, with a chord length (c) of 3 m. The rest of the rotor parameters are listed in

Table 1 of Appendix 1. The frequency peaks of the bending stress signal are plotted in Figure 2b. In the figure, the frequency peaks correspond to the wave frequency and to the second and third harmonic. We note that this scenario of only 3 wave frequencies might not be representative for operating conditions in the ocean. As such, a probabilistic approach will be evaluated in Section 3.

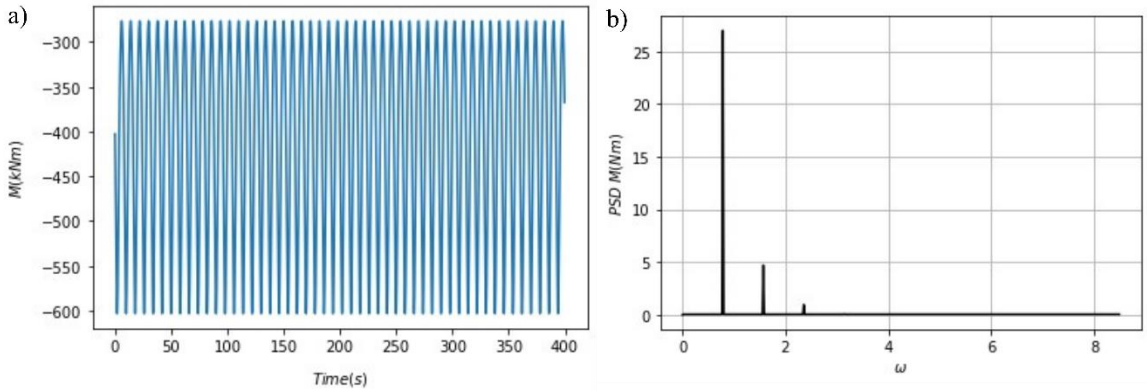

Figure 2 a) Uniform cyclic loading of a foil in a LiftWEC rotor in a regular sea state and b) frequency spectrum of bending moments in a foil of LiftWEC, subject to regular loading

Utilising uniform loading, the SN relationship is derived for specific structures or components under analysis in a laboratory setting. The SN curve is a unique relationship that varies depending on material properties or on the redundancy of the structure. Here we consider the SN curve for offshore steel in seawater with cathodic protection. In particular, we choose a D curve, whose characteristics are available in the DNV recommended practice document *Fatigue design of offshore steel structures* [4]. According to this document, the SN curve is given by

$$log\ N = log\ \bar{a} - m\ log\ \Delta\sigma \qquad [1],$$

where N is the number of cycles to failure, $\Delta\sigma$ is the stress range, m is the negative inverse slope of the SN curve and log $\bar{a}$ is the intercept of the N axis by the curve.

This project has received funding from the European Union's Horizon 2020 research and innovation programme under grant agreement No 851885. This output reflects the views only of the author(s), and the European Union cannot be held responsible for any use which may be made of the information contained therein.

We show the SN curve for offshore steel in seawater with cathodic protection in Figure 3, as defined by equation 1.

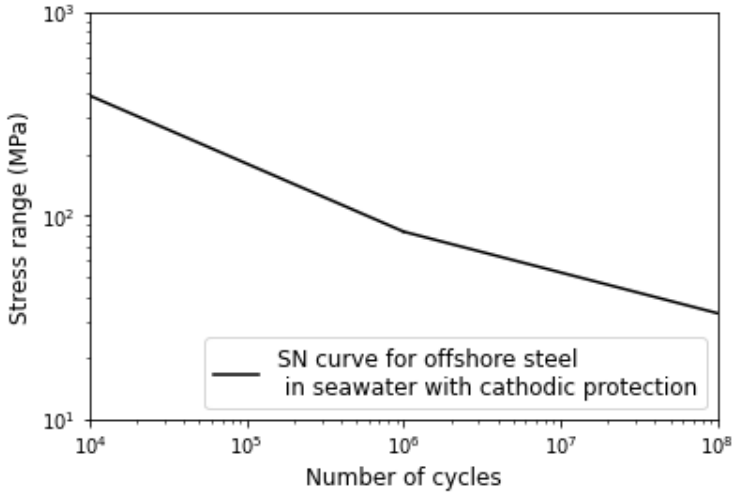

Figure 3 S-N curve for offshore steel in seawater with cathodic protection

For offshore steel, two values for $\log \bar{a}$ and m are provided. One where $N \leq 10^6$ cycles, and another one where $N > 10^6$ cycles. As an alternative to equation [1], we can describe the single slope solution for SN curves as

$$NS^m = K \qquad [2],$$

where K and m are properties of the material [5]. In the case of the SN curve of figure 3, the coefficients for equation 2 are as follows

Cycles	m	K
$N \leq 10^6$	3	5.80764E+11
$N > 10^6$	5	4.03645E+15

2.1.1 Miner's rule

To quantify the damage in a structure, Miner [6] proposed a linear summation hypothesis, where the damage D is the sum of the damage fractions of different cycles of stress ranges, i.e.

$$D = \sum_{i=1}^{n} \frac{n_i}{N_i} \qquad [3],$$

where

D is the total damage to the structure
n is the number of stress ranges
n_i is the number of cycles at stress range i
N_i is the number of cycles to failure at stress range i (from the S-N curve of the material)

This project has received funding from the European Union's Horizon 2020 research and innovation programme under grant agreement No 851885. This output reflects the views only of the author(s), and the European Union cannot be held responsible for any use which may be made of the information contained therein.

Fatigue failure occurs when $D = 1$, whilst the fatigue lifetime L is the inverse of D [5].

2.1.2 Cycle counting

Cycle counting is used in time domain methods to quantify the damage on a structure. The cycles are grouped in similar magnitude groups and the damage fractions of these cycles are added up through Miner's rule (equation 3) to quantify the total damage on the structure. One of the most popular cycle counting methods is the rainflow counting method [7]. In this type of counting, the stress time series is plotted vertically to emulate flow running down a series of pagoda roofs [5].

According to Bai et al. [5], the rainflow counting algorithm can be summarised as follows:

- CASE 1: Rainflow that starts at a valley, i.e. a minimum, should stop when it encounters rain flow coming from a lower minimum.
- CASE 2: Rainflow that starts at a peak, i.e. a maximum, should stop when it encounters rain flow coming from a more positive maximum.
- CASE 3: Rainflow stops if it meets rain from a level up.
- CASE 4: Rainflow stops at the end of the time series.

We illustrate some of these cases in Figure 4 and quantify the total number of cycles. In the figure the rain starts at the top and subsequently, inside of every peak or valley. The rain stops at the end of the time series (Case 4) or when the rain meets rain from an upper level (Case 3). A total of 4.5 cycles are quantified. We note that in Figure 4, the cycles are counted as halves (0.5) at the end of each rain flow. The end of each rain flow is highlighted with an orthogonal terminator. This example is validated with the rainflow counting libraries of Python and Matlab.

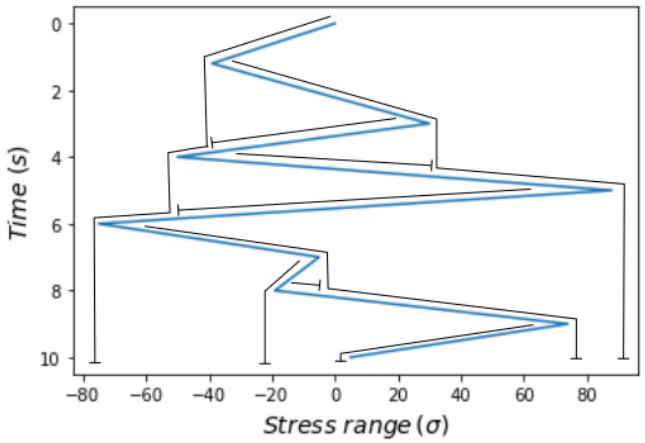

Figure 4 Rainflow cycle counting algorithm showing 4.5 cycles with cases 3 and 4 identified.

This project has received funding from the European Union's Horizon 2020 research and innovation programme under grant agreement No 851885. This output reflects the views only of the author(s), and the European Union cannot be held responsible for any use which may be made of the information contained therein.

In real sea-state operating conditions, the loading of a structure is typically of varying amplitude and phase. We illustrate this variability with an example of the radial load acting on a single foil LiftWEC device in Figure 5a. The figure shows the radial force of a single foil rotor in an interval ranging from 40 to 50 s. The measurement is part of the experimental campaign carried out in Ecole Centrale Nantes as part of the LiftWEC project. The foil is pitched at an angle of 4 degrees, the testing parameters are a wave height of H_S = 0.253 m and a wave period of T_p = 1.829 s.

The figure shows that the first two arrivals of the signal have a similar magnitude, whilst the rest of the arrivals have a lower magnitude. Although this example was measured in a laboratory setting and therefore, might not be completely representative of a real sea-state, it is useful to show the variability of the signal that a foil can encounter.

Figure 5b shows the cycles counted for the timeseries showed in Figure 5a. We note that in this example the units of the time series are Newtons. It can be seen that the low amplitude oscillations of the signal are dominant with about 60 cycles, whilst the two biggest cycles are identified to the right of the figure. It can be inferred, that for longer time series ($t > 3600\ s$), grouping the cycles and computing the damage can become a laborious task. In the next section, we present an alternative time domain approach referred to as the equivalent stress method. Then, we develop the probabilistic approach to compute damage in the selected stress hotspot.

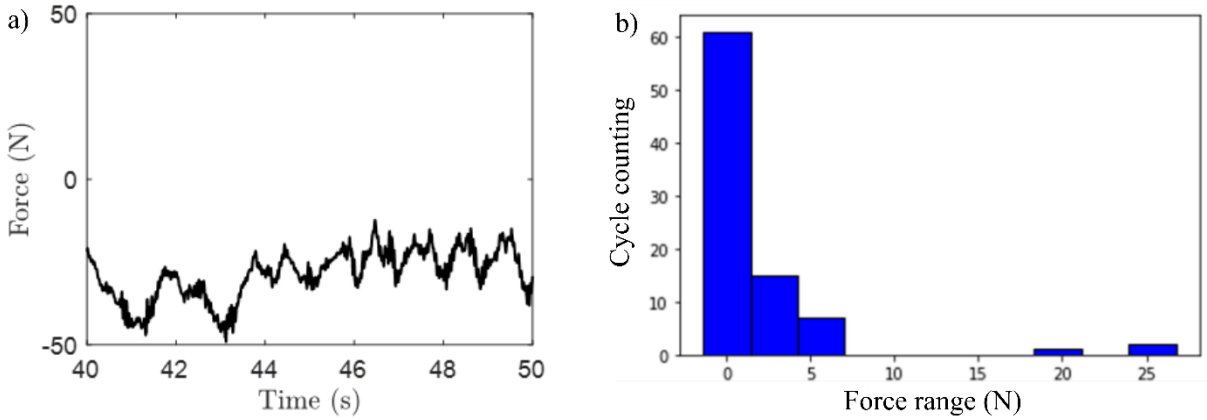

Figure 5 a) Loading on single hydrofoil LiftWEC rotor over a time interval of 40 to 50 s, where Hs = 1.829 m and Tp = 0.253 s, b) cycle counting of load time series

This project has received funding from the European Union's Horizon 2020 research and innovation programme under grant agreement No 851885. This output reflects the views only of the author(s), and the European Union cannot be held responsible for any use which may be made of the information contained therein.

2.1.3 Equivalent stress range

For variable loading, it is useful to derive an equivalent stress range S_{eq} expression to compute the damage in a structure. As such, S_{eq} is defined as

$$S_{eq} = [\sum_{i=1}^{m} \gamma_i (S_i)^{-m}]^{-1/m} \quad [4],$$

where γ_i is the proportion of the stress range S_i in the total cycle time history. A derivation of equation 4 is included in appendix 2.

Once S_{eq} is known, then we can use equation 2 to compute the equivalent number of cycles N_{eq} for that particular S_{eq}, by assuming a single slope SN curve. Then equation 3 can be used to compute the equivalent damage D_{eq} , such that

$$D_{eq} = \sum_{i=1}^{n} \frac{n_{total}}{N_{eq}} \quad [5]$$

As an example, we utilise the time series of Figure 6 to compute D_{eq} with equation 5 and D with equation 3. By defining stress ranges between 10 to 90 MPa, in intervals of 10 MPa, both D_{eq} and D result in 1×10^{-20}. The equivalent stress range is 12.41 MPa and is highlighted with the vertical dotted red lines in the figure. The equivalent stress range is low compared to the maximum stress range of the figure (approximately 70 MPa), because 33% of the cycles in this time series is within the range of 10 MPa and 32% within the range of 20 and 30 MPa. This indicates that the magnitude of the equivalent stress range will be dictated by the dominant type of cycles of the time series. In this case, the dominant type is low amplitude cycles.

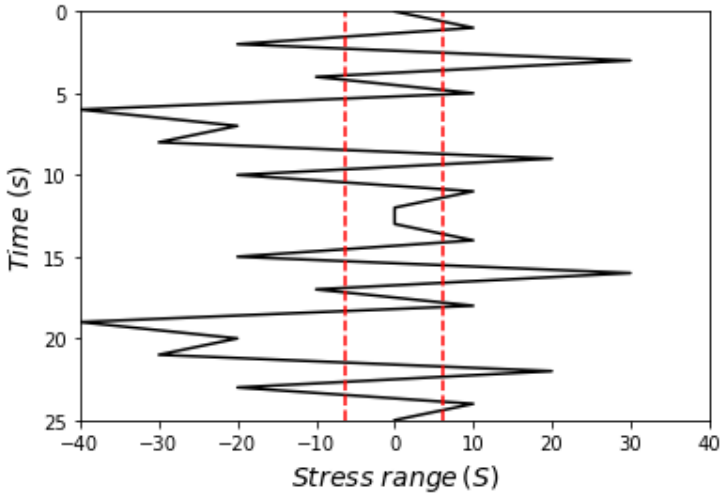

Figure 6 Example time series of stress ranges used to compute damage with equivalent stress range and with Miner's rule

This project has received funding from the European Union's Horizon 2020 research and innovation programme under grant agreement No 851885. This output reflects the views only of the author(s), and the European Union cannot be held responsible for any use which may be made of the information contained therein.

2.2 PROBABILISTIC METHODS

An irregular sea state is a statistically invariant wave condition with many different waves that can be represented by an energy spectrum. LiftWEC can operate at constant velocity in irregular sea-states. Provided that its control strategy remains constant, its spectral signature and operation could also be considered statistically invariant. This means that fatigue analysis could be performed through probabilistic methods. In fact, a probabilistic approach provides the means to capture the characteristic spectral behaviour of the loads in order to assess fatigue effects.

The operation of a LiftWEC rotor in irregular sea states and at constant velocity has been demonstrated experimentally through measurements of a two foil prototype by the LiftWEC consortium in École Centrale de Nantes, as shown with the power output of Figure 7a. In these tests, the rotor was run at the same frequency as the JONSWAP peak frequency. Future tests will investigate the optimal rotational velocity for the rotor. The operation of the rotor in an irregular sea state has also been simulated numerically. The loads on the foils are computed assuming a JONSWAP wave energy spectrum $S_{yyi}(\omega)$. The spectrum is discretised using a finite number of wave frequencies. Corresponding wave heights for each wave components are derived from the spectral density distribution. The procedure to compute discrete wave heights from a wave energy spectrum is documented for example in Jalon and Brennan, (2020) [8] and Jeans et al. (2013) [9].

The total wave-induced velocities at the foil locations are obtained by vector addition of individual wave velocity components. A constant rotational velocity of $\omega = 2\pi/T_p$ is used in the simulation. T_p refers to the peak period of the wave energy spectrum. A phase shift of 90° between rotor and peak frequency wave is maintained. We note, however, that phase effects are found to be negligible when the rotor operates in an irregular sea state. The simulated power output of the rotor tested with the conditions provided in the table of Appendix A is shown in Figure 7b. The definition of power is given in Arredondo-Galeana et al. [10]. A positive pitch angle of 2 degrees is applied to both foils.

a)

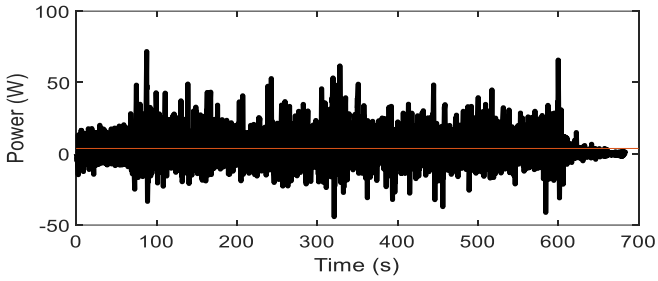

b)

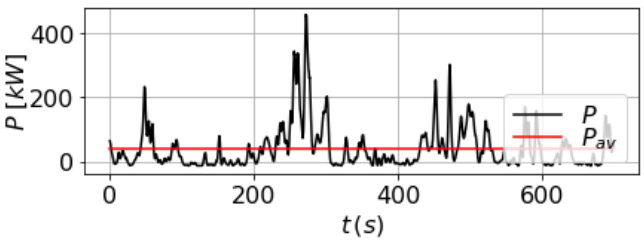

Figure 7 a) Power output of LiftWEC rotor in irregular waves as measured in Ecole Centrale Nantes and b) simulated power output in irregular waves of a a two foil rotor

This project has received funding from the European Union's Horizon 2020 research and innovation programme under grant agreement No 851885. This output reflects the views only of the author(s), and the European Union cannot be held responsible for any use which may be made of the information contained therein.

In fatigue probabilistic methods, a variable loading time series is represented by a probability density function $f_i(S)$ of the variable range S. In this case, S is the stress range and i is the i-th sea state. From Bai et al. [5], fatigue damage of an i-th sea state can be determined such that

$$D_i = \frac{n_i}{N_i} = \int_0^\infty \frac{365\times24\times3600\times P_i f_{0i} f_i(S)}{K/S_{eq}{}^m}\, dS \qquad [6]$$

where P_i is the probability of occurrence of the i-th sea state and f_{0i} is the zero-th mean frequency, such that

$$f_{0i} = (1/2\pi)\sqrt{m_{2i}/m_{0i}}, \qquad [7]$$

where m_{0i} and m_{2i}, are the zeroth and second stress spectral moments, respectively. We recall that in equation 6, S_{eq} is computed from equation 4 and K and m are obtained from a single slope SN curve of the specific material. Then, we can rewrite equation 6 as

$$D_i = A_i \int_0^\infty f_i(S)\, dS \quad [8]$$

where

$$A_i = \frac{31.536\times10^6 P_i f_{0i}}{K/S_{eq}{}^m}. \qquad [9]$$

We note that the n-th stress spectral moments of the i-th sea state are defined as

$$m_{ni} = \int_0^\infty \omega^n G_{yyi}(\omega) d\omega, \quad [10]$$

where $G_{yyi}(\omega)$ is the hot spot stress spectrum and ω is the wave frequency. From equation 10, it can be observed that the zeroth moment m_{0i} is equivalent to the area under the hot spot stress spectrum [10], such that

$$m_{0i} = \int_0^\infty G_{yyi}(\omega) d\omega, \qquad [11]$$

whilst the second stress spectral moment m_{2i} is

$$m_{2i} = \int_0^\infty \omega^2 G_{yyi}(\omega) d\omega. \quad [12]$$

In order to compute equations 11 and 12, the spectrum $G_{yyi}(\omega)$ can be obtained through the square of the Fourier transform of the hot spot stress time series. Alternatively, it can be computed from the wave spectrum of the i-th sea state $S_{yyi}(\omega)$ and the hot spot stress amplitude transfer function $H(\omega)$ for each critical part of the structure [1], such that

$$G_{yyi}(\omega) = |H(\omega)|^2 S_{yyi}(\omega). \quad [13]$$

In the analysis of this report, we consider a LiftWEC supported by a v-frame structure. We show an example of this configuration in Figure 8. From *D6.1 LW-D06-01-1x3 Extreme Event LiftWEC ULS Assessment* [3], it is known that the stress hot spots on the foils are located at the fixed ends. These hotspots are highlighted in the figure in red. The method for computing the bending stresses as a function of the distributed radial load of each foil can be found in Arredondo-Galeana et al. [11].

With the bending stresses as an input, we can then compute $G_{yyi}(\omega)$, m_{0i}, m_{2i} and f_{0i}.

This project has received funding from the European Union's Horizon 2020 research and innovation programme under grant agreement No 851885. This output reflects the views only of the author(s), and the European Union cannot be held responsible for any use which may be made of the information contained therein.

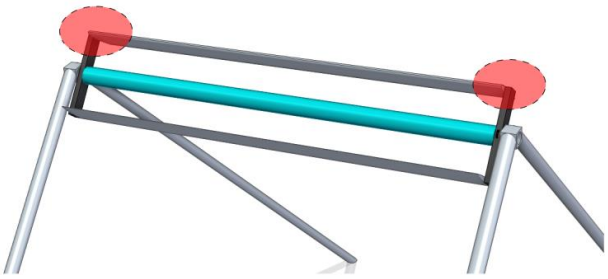

Figure 8 Three dimensional view of a two foil LiftWEC rotor, with stress hotspots highlighted in red.

In order to use equation 6, the probability of occurrence of the i-th sea state is needed. The probability of occurrence from the i-th sea state can be taken, for example, from the scatter diagram shown in Figure 9. The figure shows the wave data of the Homere database with the energy period (T_e) along the horizontal axis and the significant wave height (H_s) along the vertical axis. The scatter plot corresponds to a point in the North Atlantic at the coast of France, located at 47.84° N, 4.83° W. This location is selected because LiftWEC was originally conceived to operate in this region. The maximum probability of occurrence is at $T_e = 8$ s and $H_s = 1.5$ m, with $P = 0.018$. Because our hydrodynamic model uses the peak wave period (T_p) rather than T_e, a conversion factor between the two is needed. The conversion is performed through $T_e = \alpha T_p$, where $\alpha = 0.9$ for a JONSWAP wave spectrum [12].

In Figure 9, the total number of occurrences is 78,879. This is equivalent the total periods of 1 hours in a time interval of 9 years. This means that 1 hour intervals are considered as the duration each i-th sea state.

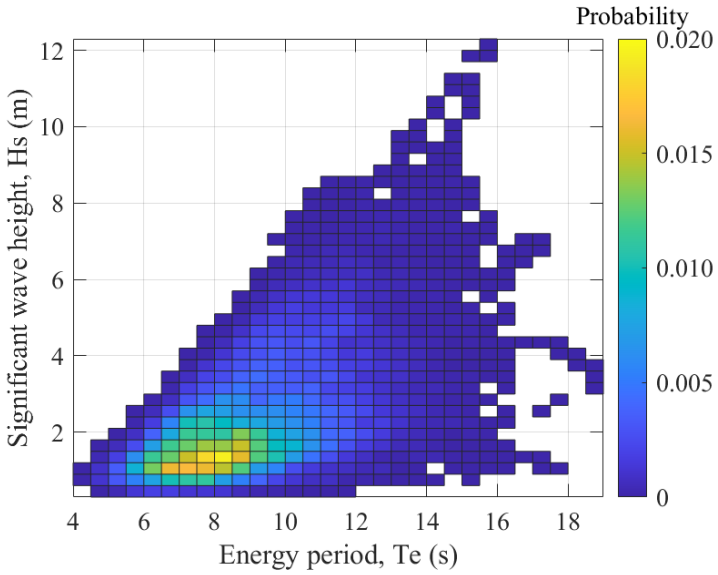

Figure 9 Probability of different sea states from HOMERE data base [13], for a point in the Atlantic coast of France.

This project has received funding from the European Union's Horizon 2020 research and innovation programme under grant agreement No 851885. This output reflects the views only of the author(s), and the European Union cannot be held responsible for any use which may be made of the information contained therein.

Typical shapes of $f_i(S)$ are shown in Figure 10. The figure shows a Rayleigh, a Weibuill and a Gamma distribution. These distributions are typically used to model the probability of occurrence of random stress ranges *[5]*. In our analysis, the area integrated under these curves in equation 6 is always 1.

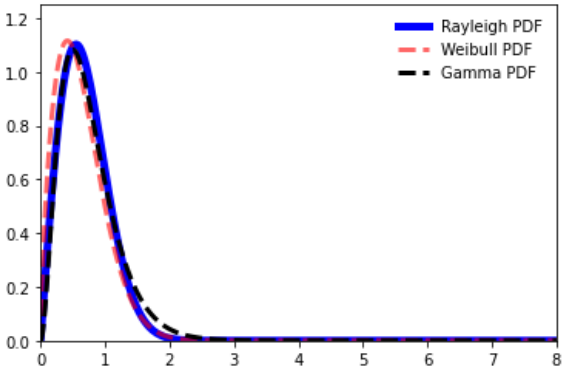

Figure 10 Stress range probability density distributions $f_i(S)$ of three different types: Rayleigh, Weibull and Gamma

To compute the damage in the hotspot, we consider a range of $5\ \text{s} \leq T_p \leq 17\ \text{s}$, with intervals of 1 s and $1\ \text{m} \leq H \leq 5\ \text{m}$, intervals of 1 m.

As an illustrative example, we compute D_i for a sea state of $H_S = 2\ \text{m}$, and $Te = 7\ s$. The computed bending stresses time series for this test case and for the selected hotspot is shown in Figure 11. The rotor parameters for the hydrodynamic loads computation are provided in Appendix 1.

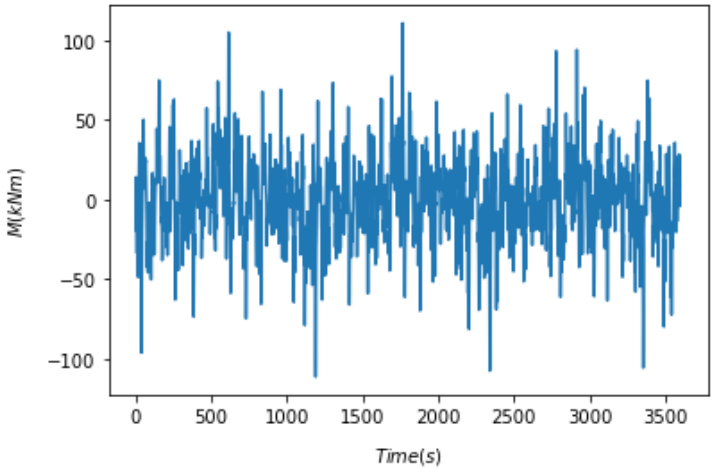

Figure 11 Hot spot stress time series in foil attachment region for $H_S = 2\ m$ and $Te = 7\ s$

This project has received funding from the European Union's Horizon 2020 research and innovation programme under grant agreement No 851885. This output reflects the views only of the author(s), and the European Union cannot be held responsible for any use which may be made of the information contained therein.

The stress hot spot power spectrum $G_{yyi}(\omega)$ is the square of the Fourier transform of the time series shown in Figure 11. To illustrate the shape similarity, both $S_{yyi}(\omega)$ and $G_{yyi}(\omega)$ are displayed in Figure 12a and Figure 12b, respectively. We select a Rayleigh distribution $f_i(S)$ to account for the probability distribution of the stress spectrum.

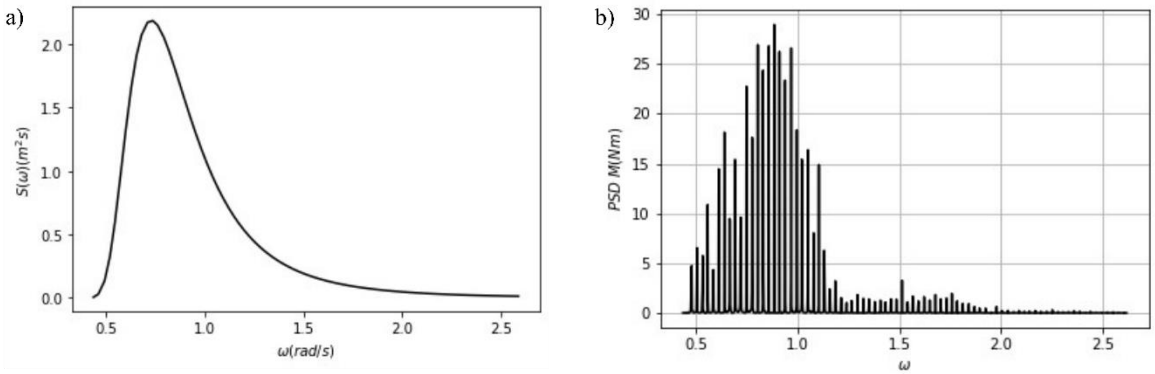

Figure 12 a) Jonswap energy spectrum $S_{yyi}(\omega)$ for the 7-th sea state and corresponding b) hotspot stress energy spectrum $G_{yyi}(\omega)$ for point in foil with maximum stresses

Assuming a probability of occurrence of 1 and a single slope SN curve with $m = 3$, the computed probabilistic damage during one hour on the hotspot is 0.0028. Comparing these results to the time series method, we observe a difference of 10%. However, this is the case only when the stress ranges do not exceed the value 83 MPa shown in figure 3. This is because the time series methods is able to capture the 2 slope curve of Figure 3, whilst the probabilistic method uses only one slope, in this case $m = 3$. We also note that the spread of the PSD has an impact on the accuracy of this comparison, and for narrower bandwidth spectra we expect the similarity between methods to converge further.

Because the similarity of computing the damage with a probabilistic and deterministic approach has been demonstrated when the stress ranges are equal or below 83 MPa, for the remaining of this report, we will use a deterministic approach and a two slope SN curve to carry out the damage computations in one hour intervals and assuming a probability of occurrence of 1 for each sea state.

This project has received funding from the European Union's Horizon 2020 research and innovation programme under grant agreement No 851885. This output reflects the views only of the author(s), and the European Union cannot be held responsible for any use which may be made of the information contained therein.

3 POWER VERSUS DAMAGE ASSESSMENT

3.1 REGULAR AND IRREGULAR SEA STATE POWER CAPTURE

It is typically expected that more power equals more damage in an energy harvesting system. Hence, for LiftWEC we firstly explore the power capture capabilities of a rotor with two foils to understand the relationship between power production and damage to the structure.

The power matrix of a LiftWEC rotor is shown in Figure 13. Figure 13a shows the power matrix in regular sea states, whilst Figure 13b shows the power matrix in irregular sea states. The horizontal axis of the figures is the peak period T_p, whilst the vertical axis is the significant wave height H_s.

The shape of the regular sea state power matrix in Figure 13a resembles the shape of a power matrix published by Siegel [14] for a cycloidal wave energy converter. The maximum power output occurs at high H_s (H_s> 4.5 m), whilst T_p is about 8 s for the testing conditions used in this study (see Appendix 1). For an irregular sea state, the power peak shifts to the right hand side to about $T_p = 11$ s, but it also occurs at H_s> 4.5 m. Although the two power matrices are not exactly the same, it is promising to see that an irregular sea state power matrix is not that dissimilar to a regular state, albeit T_p peaks at a different value. The similarity of the matrices, for example, could mean that laboratory tests could be carried out in regular sea states and empirically corrected to estimate performance in irregular sea states.

In the next section, we will compare the irregular sea state power matrix to the available power in the waves to assess the efficiency of the device in an irregular sea state (with constant rotational velocity). We then present an analysis of damage in the stress hotspot.

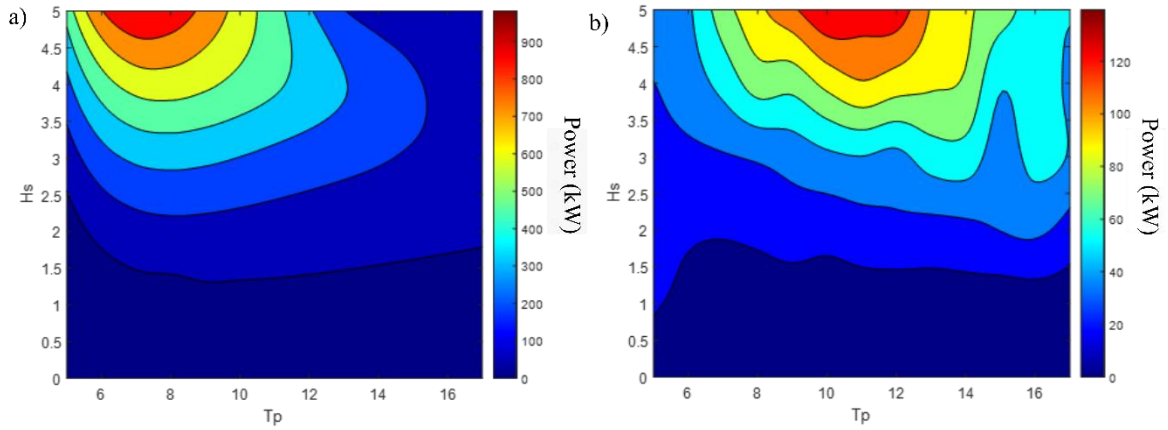

Figure 13 Power matrix of LiftWEC rotor for a) regular and b) irregular sea states

This project has received funding from the European Union's Horizon 2020 research and innovation programme under grant agreement No 851885. This output reflects the views only of the author(s), and the European Union cannot be held responsible for any use which may be made of the information contained therein.

3.2 POWER OUTPUT VERSUS DAMAGE WITH FIXED V-FRAME

We compare now the power matrix of the irregular sea state to the damage at the stress hotspot. We recall that the hotspot is the fixed end of the foil as indicated in Figure 8. The purpose of this comparison is to understand whether more power is related to more damage, as it typically occurs in wave energy extraction devices.

We compute mean power output for each of the i-th analysed sea states. The device rotates at a fixed angular velocity, which is equal to the peak angular velocity of the wave with the highest energy content in a JONSWAP energy spectrum. Time series are run for an hour in each sea state. The phase of rotation is 90 degrees with respect to the phase of the wave with maximum amplitude in the spectrum. Although we note that in an irregular sea state, in contrast to a regular sea state, the effect of the phase does not impact the power output of the device.

Figure 15a and Figure 15b show P_i and D_i, respectively. The latter is computed with equation 3 and the computation is verified through the equivalent stress range method of Section 2.4. In the figures, the sea states are interpolated to 100 points to smooth the contour plot. Figure 15a shows that the peak P_i occurs at $T_p = 11$ s. The power decreases for longer and shorter waves. It can also be seen that the highest P_i occurs at high amplitude waves, in this case when Hs = 5 m. In contrast, Figure 15b shows that the peak in D_i is detected at $T_p = 6.2$ s and Hs = 5 m. At the same wave amplitude but to the left hand side of the peak in P_i peak.

This shows that for a LiftWEC rotor highest power does not necessarily translate into the highest damage. This could be because at smaller periods, the number of cycles increases. Furthermore, the power production depends on the tangential force of the foil, whilst the damage depends on the radial force acting on the foil. When lift and drag forces are high, both contribute positively and increase the damage on the structure. In this scenario, the power drops because the tangential component of the drag force reduces the effective component of the lift force to drive the rotor. In contrast, when the drag decreases, the power production increases, because more effective lift force drives the rotor. At the same time less damage occurs on the structure because the effect of the drag acting normal to the foil is minimal.

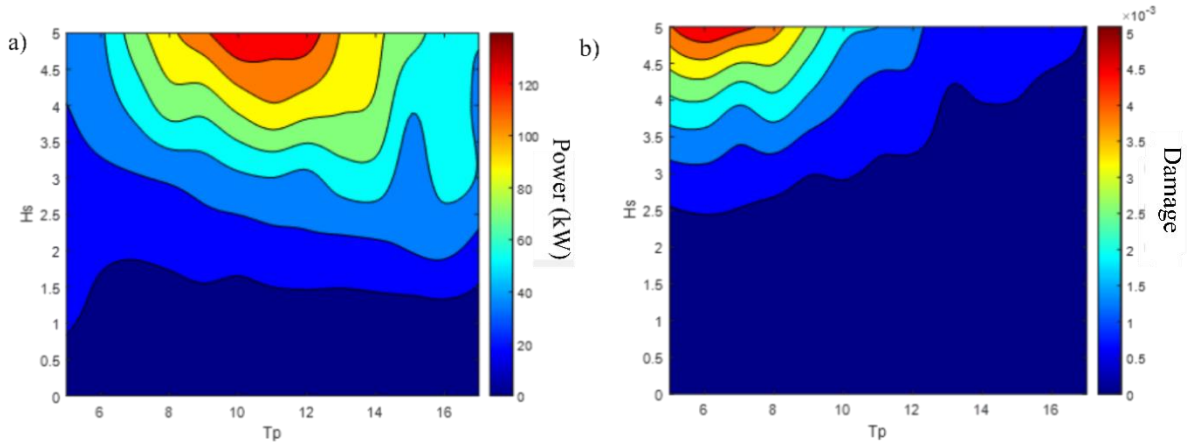

Figure 14 a) Power and b) damage contour plot of LiftWEC rotor with a rigid v-frame or a rigid tensioned legged support structure

This project has received funding from the European Union's Horizon 2020 research and innovation programme under grant agreement No 851885. This output reflects the views only of the author(s), and the European Union cannot be held responsible for any use which may be made of the information contained therein.

3.3 POWER OUTPUT VERSUS DAMAGE WITH V-FRAME STRUCTURE

The effect of compliance of a v-frame structure in the power output and in the damage is demonstrated in this section. The compliant v-frame structure is shown in figure 16. The figure is representative of a v-frame structure or equally of a structure moored with tension lines. The supports of the structure are modelled as springs as depicted in the figure. We note that the effect of compliance in this type of structure should be similar to that of the floating configuration attached to a tri-floater, since the motion is expected to be driven by the radial forces in a similar manner, in both the v-frame and tri-floater structure. The hotspot to analyse the damage is one of the fixed ends of the foil. The rotor is driven at constant rotational velocity, i.e. the peak frequency of the wave spectrum.

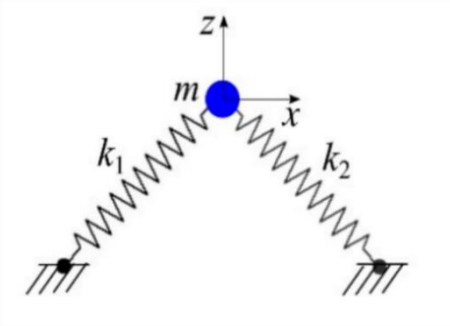

Figure 15 V-frame or tension legged structure with compliance for a LiftWEC rotor

Figure 17a and Figure 17b show P_i and D_i, respectively for the compliant structure. In the figures, the sea states are interpolated to 100 points to smooth the contour plot. Figure 17a shows that the peak P_i occurs at $T_p = 9.5$ s and at Hs = 5 m. The power decreases for longer and shorter waves, and for lower wave heights. In terms of damage, Figure 16b shows that the peak in D_i is at $T_p = 6.2$ s and at Hs = 5 m. The results are similar for both P_i and D_i to those found with a rigid support structure, and no significant difference in power performance is observed. The magnitude of the maximum damage increases slightly at the fixed end of the foil, but the general footprint of the damage matrix is similar to that of the fixed case. The increase in damage in the foil hotspot could be due to the exposure of the foil to higher loads as it moves slightly away compared to the trajectory of a foil in a fixed v-frame structure. However, this increment is small, and it is expected that at the anchoring points of the structure, compliance could actually reduce the damage on it.

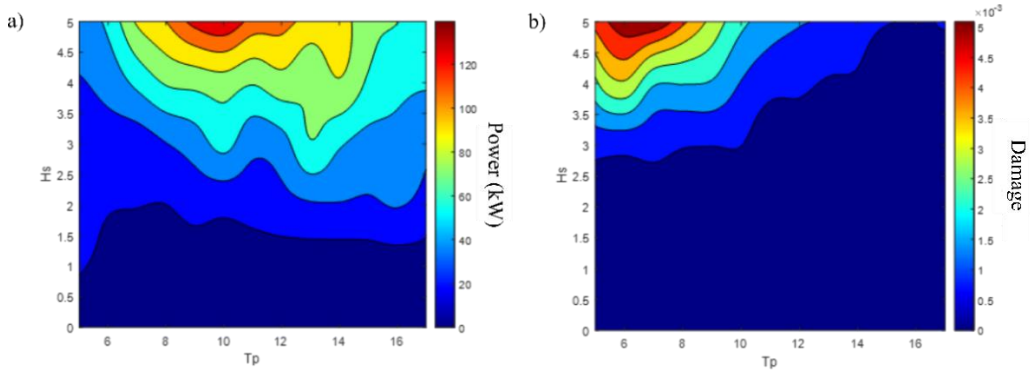

Figure 16 a) Power and b) damage contour plot of LiftWEC rotor with a compliant v-frame or a compliant tensioned legged support structure

This project has received funding from the European Union's Horizon 2020 research and innovation programme under grant agreement No 851885. This output reflects the views only of the author(s), and the European Union cannot be held responsible for any use which may be made of the information contained therein.

3.4 POWER OUTPUT VERSUS DAMAGE WITH PASSIVE RADIAL MOTION

In deliverable *D6.3 Structural Dynamic Model Development* [15], we showed that in a two foil LiftWEC rotor, compliance of one of the foils can increase power extraction. In this section we will explore the effect of passive radial compliance in the damage experienced by the rotor in the selected hotspot. Radial heaving is expected to increase the damage on the rotor due to the increase in power extraction. Figure 18 shows the two passive mechanisms represented with a compressional and a torsional spring in one of the foils of a LiftWEC rotor.

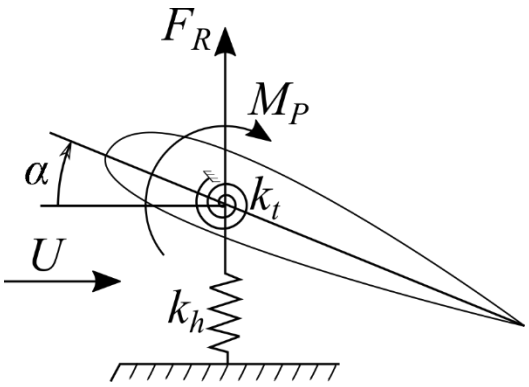

Figure 17 Single foil representation of a LiftWEC rotor with passive heaving and pitching compliance.

Figure 19a and Figure 19b show P_i and D_i, respectively for the radial heaving case. In the figures, the sea states are interpolated to 100 points. The figures show similar footprint as those corresponding to the fixed and compliant structure. We recall that the main effect of the passive radial motion in a regular sea state is to increase the power extracted in the device [15]. In this example, the areas of extracted power increase slightly downwards of Figure 19a, in agreement to the regular sea state findings. The damage plot of Figure 19b shows that the maximum damage on the structure increases slight compared to the fixed v-frame case. However, the general footprint of the damage matrix does not show a major difference to the previous cases. As such, radial heaving is recommended as a mechanism to increase power extraction without incurring in a significant structural penalty.

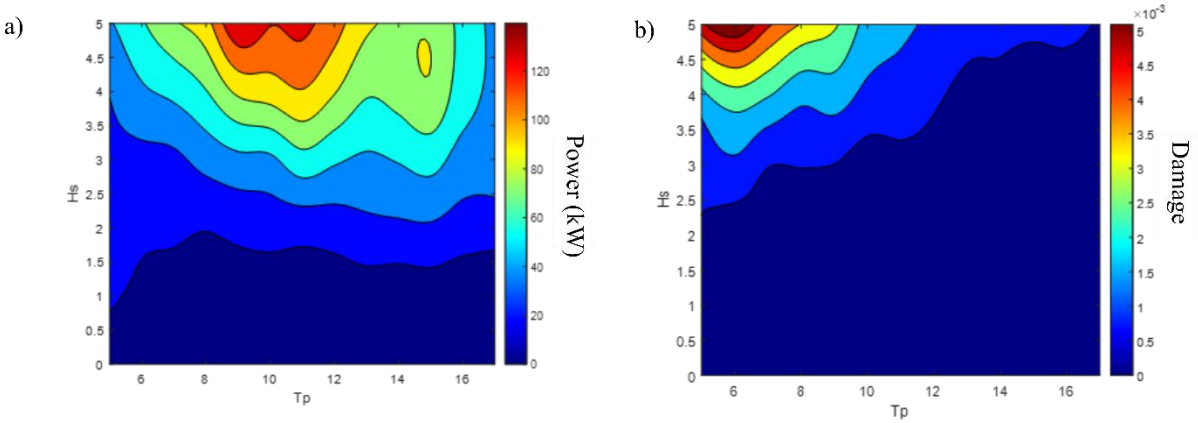

Figure 18 a) Power and b) damage contour plot of LiftWEC rotor with a compliant radial heaving

This project has received funding from the European Union's Horizon 2020 research and innovation programme under grant agreement No 851885. This output reflects the views only of the author(s), and the European Union cannot be held responsible for any use which may be made of the information contained therein.

3.5 POWER OUTPUT VERSUS DAMAGE WITH PASSIVE PITCH

In this section, the effect of passive foil pitching compliance is explored. It is expected that passive pitching compliance will alleviate peak loading and therefore decrease damage on the rotor. The equilibrium state of the model is shown in Figure 20a. This state occurs when the foil rotates around the central shaft in the absences of waves. Because the foil is free to pitch at its leading edge and has a torsional spring attached to the pitching axis, the hydrodynamic moment (M_h) is balanced by the torsional moment (M) [16]. The hydrodynamic moment occurs due to lift force that occurs due the rotation of the foil.

Because the torsional moment and the hydrodynamic moments are in equilibrium, any flow disturbance will pitch the foil to another equilibrium position (Figure 20b) due to a change in the lift force (δL) and in the hydrodynamic moment (δM_h). If the stiffness of the spring is properly tuned, the angle of attack on the foil will decrease on the foil. This is shown in Figure 19b. The new equilibrium position reduces or cancels the change in the inflow disturbance when $\delta\alpha = \delta\theta$.

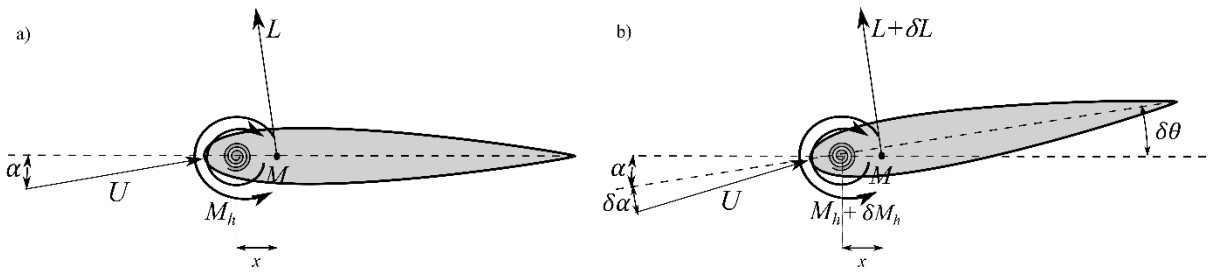

Figure 19 a) Passively pitching foil in equilibrium position with inflow U b) Passively pitching foil deflected by θ after change in U and sustaining α as in the equilibrium position

The equation of motion of the torsional spring is

$$M = k\theta \quad [12]$$

where k is the spring constant and θ is the preload angle of the spring. In order to sustain a fixed angle of attack, the hydrodynamic moment of the foil M_h is equal to the torsional moment M, such that

$$M = k\theta = xL \qquad [13],$$

where L is the lift force and x is the distance between the pitching axis and the quarter chord coordinate of the foil. The pitch displacement can be computed rearranging equation 13, such that

$$\delta\theta = \frac{x\delta L}{k} \qquad [14].$$

In order to compute the new angle of attack (α_n) after the foil deformation, we compute first the angle of attack α_{t+1} that the foil experiences without any pitch at $t+1$ (Figure 20b). Then, the inflow disturbance $\delta\alpha$ at $t+1$ is

$$\delta\alpha = \alpha_{t+1} - \alpha_t, \quad [15]$$

where t denotes a time index and α_t is the initial angle of attack (Figure 20a). Once $\delta\alpha$ and α_{t+1} are known, we can compute the foil $\delta\theta$ with equation 14.

This project has received funding from the European Union's Horizon 2020 research and innovation programme under grant agreement No 851885. This output reflects the views only of the author(s), and the European Union cannot be held responsible for any use which may be made of the information contained therein.

Lastly, α_n can be computed as

$$\alpha_n = \alpha_t + \delta\alpha - \delta\theta. \text{ [16]}$$

We can now compute the resulting radial forces due to a passively pitching foil and evaluate the damage in the structure.

Results for the passively pitching foil power output and damage in irregular sea states are show in Figure 20a and Figure 20b, respectively. For both foils, we select a spring stiffness that produces a 10% power drop in a regular sea state. This stiffness was selected because it was found to be provide a significant damage reduction and only a slight loss in average power in a regular sea state scenario.

In an irregular sea state, the power output of Figure 20a shows that the power performance of the rotor does not reach the same level as that of the system with rigid foils. The peak power is about 20% less to that found for the rigid foil case. The damage, however, shows a significant reduction compared to that of a rigid foil two-rotor system. This type of passively pitching mechanism could be useful for offshore long term operations. The system could be further optimised for spring stiffness by tuning a unique stiffness for each foil, and also tuning the stiffness in terms of power output. This is a topic of further research within the LiftWEC consortium.

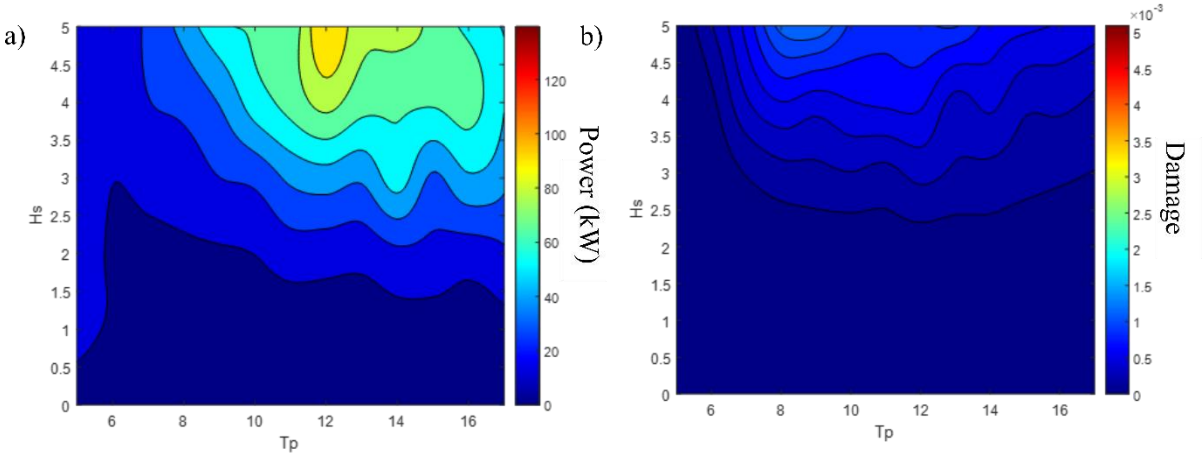

Figure 20 a) Power and b) damage contour plot of LiftWEC rotor with passive pitch in irregular waves

This project has received funding from the European Union's Horizon 2020 research and innovation programme under grant agreement No 851885. This output reflects the views only of the author(s), and the European Union cannot be held responsible for any use which may be made of the information contained therein.

4 CONCLUSIONS

This deliverable D6.4 Fatigue Assessment presents the foundations for fatigue and damage analysis in the LiftWEC device. The fatigue and damage analysis can be carried out through three methods: 1) time series analysis, 2) equivalent stress range method and 3) probabilistic method. In this work, we demonstrate the use of the three methods for the analysis of an example stress hotspots. This hotspot is the fixed end of the foils. The analysis, however, is applicable to any other stress hotspot provided that a stress time series analysis is available. We note that the results section of this deliverable utilises the fatigue time deterministic methods, since the probabilistic method was only applicable for single SN curve scenarios, i.e. when the stress ranges of the hotspot did not exceed 83 MPa.

It is typically expected that more power reflects in more damage on a structure, because larger forces induce more damage. In our hotspot example, this was found not to be the case. This is because the power of the LiftWEC device is proportional to the tangential forces on the foils, whilst the damage is proportional to the radial forces that generate the bending moments. In contrast, the shape of the damage matrix is expected to have more resemblance to the power matrix in hotspots where the tangential forces are the source of damage to the structure, i.e. the shaft of the rotor.

We have also explored the effect of the support structure compliance, radial and pitching compliance of the foils. For the conditions considered in this work, we found that compliance of the structure and passive heaving of the foil do not alter significantly the damage on the structure. We note, however, that passive heaving does seem to reflect a slight increase in power output, as observed in regular sea states in D6.3 Structural Dynamic Model [15]. In contrast, passive pitch shows a significant reduction in fatigue damage, although at a slight drop of power production (peak power drops about 20%). The passive pitching mechanism, however, can be optimised for specific stiffnesses in each foil and for power production.

The tools developed in this deliverable are expected to be used as a methodology to assist the life design of a LiftWEC device subject to irregular sea states. The results are novel by showing that for certain hotspots, such as the fixed ends of the foils, the damage and the power follow different patterns due to their association to the different radial and tangential forces that are generated in the foils. It is also the first time, that passively compliance in the support structure and the foils is explored as means of a control strategy to enhance power and mitigate fatigue damage.

This project has received funding from the European Union's Horizon 2020 research and innovation programme under grant agreement No 851885. This output reflects the views only of the author(s), and the European Union cannot be held responsible for any use which may be made of the information contained therein.

5 BIBLIOGRAPHY

[1] F. P. Brennan, Fatigue and fracture mechanic analysis of threaded connections, London : University College London, 1992.

[2] L. P. Pook, The role of crack growth in metal fatigue, London: The Metals Society, 1982.

[3] A. Arredondo-Galeana, W. Shi and F. Brennan, "LiftWEC: D6.1 Extreme Event LiftWEC ULS Assessment," 2020.

[4] "RECOMMENDED PRACTICE DNV-RP-C203. FATIGUE DESIGN OF OFFSHORE STEEL STRUCTURES," DNV, 2010.

[5] X. Bai, Y. Zhao, G. Dong and C. Bi, "Probabilistic analysis and fatigue life assessment of floating collar of fish cage due to random wave loads," *Applied Ocean Research,* vol. 81, pp. 93-105, 2018.

[6] M. A. Miner, "Cumulative Damage in Fatigu," *J. Appl. Mech,* vol. 12, no. 3, pp. A159-A164 , 1945.

[7] M. a. T. E. Matsuichi, "Fatigue of metals subjected to varying stress," in *Japan Society of Mechanical Engineering*, Fukuoka, 1968.

[8] M. L. Jalón and F. Brenan, "Hydrodynamic efficiency versus structural longevity of a fixed OWC wave," *Ocean Engineering,* 2021.

[9] T. Jeans, C. Fagley, S. Siegel and J. Seidel, "Irregular deep ocean wave energy attenuation using a cycloidal wave energy converter," *International Journal of Marine Energy,* pp. 16-32, 2013.

[10] Y. Bai and W.-L. Jin, Marine Structural Design (Second Edition), Butterworth-Heinemann, 2016.

[11] A. Arredondo-Galeana, W. Shi, G. Olbert, M. Scharft, A. Ermakov, J. V. Ringwood and F. Brennan, "A methodology for the structural desing of LiftWEC: A wave-bladed cyclorotor," in *European Wave and Tidal Energy Conference (EWTEC)*, Plymouth, 2021.

[12] A. M. Cornet, "A global wave energy resource assessment," in *The Eighteenth International Offshore and Polar Engineering Conference*, Vancouver, Canada, 2008.

[13] M. Accensi and C. Maisondieu, "HOMERE. Ifremer - Laboratoire Comportement des Structures en Mer.," 2015.

[14] S. G. Siegel, "Numerical benchmarking study of a Cycloidal Wave Energy Converter," *Renewable Energy,* vol. 134, pp. 390-405, 2019.

This project has received funding from the European Union's Horizon 2020 research and innovation programme under grant agreement No 851885. This output reflects the views only of the author(s), and the European Union cannot be held responsible for any use which may be made of the information contained therein.

[15] A. Arredondo-Galeana, W. Shi and F. Brennan, "LiftWEC: D6.3 Structural Dynamic Model Development," 2021.

[16] A. Arredondo-Galeana, A. M. Young, A. S. M. Smyth and I. M. Viola, "Unsteady load mitigation through a passive trailing-edge flap," *Journal of Fluids and Structures,* vol. 106, no. 103352, 2021.

[17] J. Schijve, Fatigue of Structures and Materials, Springe Science & Business Media, 2001.

[18] F. P. Brennan, "A framework for variable amplitude corrosion fatigue materials tests for offshore wind steel support structures," *Fatigue & Fracture of Engineering Materials & Structures,* 2014.

[19] T. Jeans, C. Fagley, S. Siegel and J. Seidel, "Irregular deep ocean wave energy attenuation," *International Journal of Marine Energy,* vol. 1, pp. 16-32, 2013.

6 APPENDIX 1

It is important to specify the operational and structural parameters of LiftWEC used in the structural dynamic model. We identify the following parameters of importance: Rotor radius (r), submergence (μ), chord length (c), span (s), angular frequency (ω), phase difference ($\Delta\varphi$), mass of hydrofoil (kg), significant wave height (H_s) and peak period (T_p). The values utilised in this deliverable for each of these parameters are provided below in Table 1.

Parameter	Modelled value
Rotor radius (r)	6 m
Submergence (μ)	-12 m
Chord length (c)	4 m
Span (s)	10 m
Angular frequency (ω)	0.6283 rad/s
Phase difference ($\Delta\varphi$)	Hydrofoil 1: +90°, Hydrofoil 2: -90°
Mass of hydrofoil (kg)	15 tonnes

Table 1 Relevant operational and structural parameters of rotor

This project has received funding from the European Union's Horizon 2020 research and innovation programme under grant agreement No 851885. This output reflects the views only of the author(s), and the European Union cannot be held responsible for any use which may be made of the information contained therein.

7 APPENDIX 2

The equivalent stress range S_{eq} derivation is presented in this section. By equating the damage due to a hypothetical S_{eq} to the damage computed through the sum of the i-th damages due to the i-th cycles, we get

$$D = \frac{n_{Total}}{A\Delta S_{eq}^{m}} = \frac{1}{A}\left[\sum_{i=1}^{k} \frac{n_i}{(\Delta S_i)^m}\right],$$

where n_{Total} is the total number of cycles, A is a constant computed from the SN curve, ΔS_{eq} is the equivalent stress range, m is the slope of the SN curve, k is the upper limit of the summation and equals to the total number of cycles, n_i is the i-th cycle and ΔS_i is the i-th stress range.

We can rearrange the left hand side of the above equation, such that:

$$A^{-1}\Delta S_{eq}^{-m} = \frac{1}{A}\left[\sum_{i=1}^{k} \frac{n_i}{n_{Total}} (\Delta S_i)^{-m}\right],$$

then solving for the ΔS_{eq}, we obtain

$$\Delta S_{eq} = \left[\sum_{i=1}^{k} \gamma^i (\Delta S_i)^{-m}\right]^{\frac{-1}{m}},$$

where γ is the proportion of stress ranges.

This project has received funding from the European Union's Horizon 2020 research and innovation programme under grant agreement No 851885. This output reflects the views only of the author(s), and the European Union cannot be held responsible for any use which may be made of the information contained therein.